Published in final edited form as:

Biomaterials. 2014 October ; 35(30): 8585–8595. doi:10.1016/j.biomaterials.2014.06.057.

ECM hydrogel coating mitigates the chronic inflammatory response to polypropylene mesh

Denver M. Faulk[a,b], **Ricardo Londono**[b,c], **Matthew T. Wolf**[a,b], **Christian A. Ranallo**[a,b], **Christopher A. Carruthers**[a,b], **Justin D. Wildemann**[a,b], **Christopher L. Dearth**[b,d], and **Stephen F. Badylak**[a,b,d,*]

[a]Department of Bioengineering, University of Pittsburgh, 450 Technology Drive, Suite 300, Pittsburgh, PA, USA

[b]McGowan Institute for Regenerative Medicine, University of Pittsburgh, 450 Technology Drive, Suite 300, Pittsburgh, PA, USA

[c]School of Medicine, University of Pittsburgh, 450 Technology Drive, Suite 300, Pittsburgh, PA, USA

[d]Department of Surgery, University of Pittsburgh, 450 Technology Drive, Suite 300, Pittsburgh, PA, USA

Abstract

Polypropylene has been used as a surgical mesh material for several decades. This non-degradable synthetic polymer provides mechanical strength, a predictable host response, and its use has resulted in reduced recurrence rates for ventral hernia and pelvic organ prolapse. However, polypropylene and similar synthetic materials are associated with a chronic local tissue inflammatory response and dense fibrous tissue deposition. These outcomes have prompted variations in mesh design to minimize the surface area interface and increase integration with host tissue. In contrast, biologic scaffold materials composed of extracellular matrix (ECM) are rapidly degraded in-vivo and are associated with constructive tissue remodeling and minimal fibrosis. The objective of the present study was to assess the effects of an ECM hydrogel coating on the long-term host tissue response to polypropylene mesh in a rodent model of abdominal muscle injury. At 14 days post implantation, the ECM coated polypropylene mesh devices showed a decreased inflammatory response as characterized by the number and distribution of M1 macrophages (CD86+/CD68+) around mesh fibers when compared to the uncoated mesh devices. At 180 days the ECM coated polypropylene showed decreased density of collagen and amount of mature type I collagen deposited between mesh fibers when compared to the uncoated mesh devices. This study confirms and extends previous findings that an ECM coating mitigates the chronic inflammatory response and associated scar tissue deposition characteristic of polypropylene.

*Corresponding author. Department of Bioengineering, University of Pittsburgh, 450 Technology Drive, Suite 300, Pittsburgh, 15219 PA, USA. Tel.: +1 412 624 5253; fax: +1 412 624 5256. badylaks@upmc.edu (S.F. Badylak).

Keywords

ECM (extracellular matrix); Hydrogel; Surgical mesh; Polypropylene; Coated surgical mesh; Foreign body response

1. Introduction

Polypropylene (PP), polyethylene, and polyethylene terephthalate (PET) are the most commonly used non-degradable synthetic mesh materials for abdominal and inguinal hernia repair [1,2], and knitted polypropylene is now the most frequently used material for ventral hernia repair [3]. Polypropylene's robust mechanical properties and beneficial effect upon the repair of ventral hernia and pelvic organ prolapse is well documented, but the host soft tissue response is characterized by chronic inflammation and dense fibrous connective tissue deposition [4–8].

Biologic scaffolds composed of allogeneic or xenogeneic ECM have been used to reconstruct a variety of tissues including the skin [9], body wall [10,11], urinary bladder [12], and rotator cuff [12] among others. ECM scaffolds have become increasingly attractive for hernia repair because of their ability to abrogate the foreign body response, prevent infection, and minimize or avoid excessive fibrosis [2,13,14]. ECM scaffold degradation releases potent bioactive matricryptic peptides [15–19] that promote angiogenesis, chemotaxis, mitogenesis, and cellular differentiation during the constructive remodeling process [17,20]. Though ECM scaffolds have been shown to promote the deposition of site appropriate soft tissue such as muscle tissue [21,22], adipose tissue, and/or vascularized reticular connective tissue rather than dense fibrous tissue [23], a loss of mechanical strength during degradation has limited its use in hernia repair.

The development of a surgical mesh device that integrates the robust mechanical properties of polypropylene with the desirable tissue remodeling properties of the naturally occurring ECM can have significant clinical application. A method to coat a synthetic polypropylene hernia mesh with ECM has previously been described [24]. The resulting hybrid mesh was shown to alter the default acute host response to the polypropylene mesh by delaying and reducing the accumulation of pro-inflammatory foreign body giant cells. This response was associated with a suppression of the proinflammatory M1 macrophage phenotype at the polypropylene/ host tissue interface. The new host tissue deposition was altered after 35 days. The pores in the ECM coated mesh were filled with loose connective tissue rather than the dense, large fiber collagenous tissue noted in the uncoated mesh material pores. These differences in remodeling were associated with no loss of biaxial mechanical strength. Nonetheless, it is unknown whether these favorable outcomes persist in the long term well after the ECM component had fully degraded. The objective of the present study was to assess the long term in vivo remodeling response and biomechanics in a rat partial thickness abdominal wall defect model. The study investigated the host response to both heavy-weight and light-weight polypropylene meshes coated with porcine dermal ECM.

2. Materials and methods

2.1. Experimental overview

Test devices included uncoated and ECM coated heavy-weight BARD™ polypropylene mesh (C.R. BARD, city, state), uncoated and ECM coated light-weight BARD™ Soft polypropylene mesh (C.R. BARD), and uncoated light-weight Ultra-Pro™ mesh (Ethicon.). These devices were implanted in a previously described [24–26] rat partial thickness bilateral abdominal defect overlay model. The two time points investigated were 14 and 180 days. Histomorphologic scoring of the tissue remodeling response as well as macrophage phenotype characterization were performed at 14 days. Histomorphologic assessment, collagen deposition characterization, and biaxial testing were performed at 180 days post implantation. A total of 80 mesh devices were implanted, and 40 animals were used over the course of the study (i.e., bilateral implants per animal); 20 mesh devices were implanted for the 14 day time point (n-value = 4 for each device), 60 mesh devices were implanted for the 180 day time point (n-value = 12 for each device, 8 for biaxial testing and 4 for histology).

2.2. ECM preparation and polypropylene mesh coating

Dermal ECM was prepared as previously described [24]. Briefly, full thickness skin was harvested from market weight (~110 kg) pigs (Tissue Source, Inc., Lafayette, IN) and the subcutaneous fat and epidermis were removed by mechanical delamination followed by treatment with 0.25% trypsin (Thermo Fisher Scientific, Waltham, MA) for 6 h, 70% ethanol for 10 h, 3% H_2O_2 for 15 min, 1% Triton X-100 (Sigma–Aldrich, St. Louis, MO) in 0.26% EDTA/0.69% Tris for 6 h with a solution change for an additional 16 h, 0.1% peracetic acid/4% ethanol (Rochester Midland, Rochester, NY) for 2 h. Water washes were performed between each chemical change with alternating water and phosphate buffered saline (PBS) washes following the final step. All chemical exposures were conducted under agitation on an orbital shaker at 300 rpm. Dermal ECM was then frozen, lyophilized, and comminuted into a 40 mesh powder. The dermal ECM powder was solubilized as previously described [27] by partial enzymatic digestion in a 1 mg/mL pepsin (Sigma–Aldrich) solution in 0.01 N HCl for 48 h at a concentration of 10 mg ECM/mL solution (dry wt/vol). Solubilized dermal ECM was brought to physiologic pH and salt concentration while on ice by adding 1/9 the digest volume of 10X PBS, 1/10 the volume of 0.1 N NaOH, and then further diluted to 8 mg ECM/mL with 1X PBS.

The neutralized dermal ECM digest was immediately added to a square plastic dish and 2 cm × 3 cm pieces of pre-cut polypropylene mesh were suspended in the solution. The neutralized digest and polypropylene mesh were then placed in a non-humidified incubator at 37 °C for approximately 30–45 min until the dermal ECM digest formed a hydrogel (~4.5 mm total thickness) around the mesh and between the fibers of the polypropylene mesh. The dermal ECM hydrogel embedded mesh was then air dried at 37 °C overnight to complete the coating process. The end coating is a very thin (<1 mm) solid film around the synthetic mesh. This solid film will flake or chip if the mesh is bent at extreme angles while in a completely dry form. However, the ECM coating becomes pliable within minutes of hydration with saline or distilled water, and did not flake or chip during regular handling. All devices used for in vivo implantation were terminally sterilized with ethylene oxide.

2.3. Surgical model and mesh implantation

All procedures were approved by and performed according to the guidelines of the Institutional Animal Care and Use Committee at the University of Pittsburgh (protocol #12111053). Anesthesia was induced with 2.5–4% isoflurane, and surgical plane anesthesia was maintained with 0.5–4% isoflurane throughout the procedure. The ventral abdomen was prepared for aseptic survival surgery by clipping the fur over the entire abdominal region, and cleaning the operative area with three alternating scrubs of providone-iodine surgical scrub and 70% isopropyl alcohol solutions. A final preparation of 70% isopropyl alcohol was applied and allowed to dry, followed by placing sterile surgical drape(s) over the entire field. Following preparation of the ventral abdomen, a midline skin incision was made, and the skin on the right side of the abdomen was bluntly dissected from the underlying muscular tissue. A 1 cm^2 partial thickness defect was created by removing the internal and external oblique, leaving the transversalis fascia and the peritoneum intact. A 2 cm × 3 cm surgical mesh test article was then fixated directly over top of the defect (i.e., overlay technique) using six (6) interrupted 4-0 PROLENE™ sutures (Fig. 1). Following placement of the test article, the skin was closed with a continuous 4-0 VICRYL™ suture. A 1 cm^2 partial thickness defect with mesh overlay was then performed on the left side in a similar manner as the right. The animal was recovered from anesthesia, returned to its cage and allowed free access to food and water *ad libitum*. Rats were given Buprenex® (0.06 mg/kg subcutaneously) and Baytril® (5 mg orally) at the time of surgery and for 3 days post-surgery. Four (4) mesh devices from each group were explanted per time point to evaluate the histolomorphologic response, with an additional eight (8) mesh devices from each group explanted for 180 day biaxial mechanics testing.

2.4. Test article collection

At 14 days or 180 days post implantation, animals were sacrificed and test articles were excised with adjacent normal tissue. Euthanasia was achieved by CO_2 inhalation and subsequent cervical dislocation, which was performed in accordance with the guidelines of the American Veterinary Medical Association (AVMA) Panel of Euthanasia, and Journal of the American Veterinary Medical Association, 218(5):668–696, 2001. Following euthanasia, the skin was gently dissected, reflected, and photographs were taken of each animal and each test or control article in situ (Fig. 2). The sample was then divided in half and each half immersed in 10% Neutral Buffered Formalin (NBF) for further histological analysis.

2.5. Assessment of macrophage phenotype

Mesh devices were explanted 14 days post implantation, along with surrounding abdominal wall tissue. Mesh/tissue explants were fixed with 10% neutral buffered formalin for at least 24 h, embedded in paraffin, and sectioned (5 μm). Immunoflourescent labeling was performed to characterize macrophage phenotype in response to ECM coated and uncoated polypropylene mesh test articles. Slides were deparaffinized followed by antigen retrieval in heated citrate buffer for 20 min (10 m_M citrate, pH 6.0 at 95–100 °C). Non-specific antibody binding was prevented by incubation for 1 h at room temperature with a blocking solution consisting of 2% normal horse serum (Hyclone), 1% bovine serum albumin (Sigma), 0.1% Triton X-100 (Sigma), and 0.1% Tween-20 (Sigma) in PBS. Sections were decanted and

incubated with primary antibodies diluted 1:150 in blocking solution overnight at 4 °C. Primary antibodies against the pan-macrophage marker CD68 (mouse anti-rat CD68, clone ED1, Abd Secotec), the M1 macrophage marker CD86 (rabbit anti-human CD86, clone EP 1158Y, Abcam), and the M2 macrophage marker CD 206 (goat anti-human CD206 goat anti-human CD206, polyclonal, Santa Cruz) were used. Sections were washed and incubated with the following fluorescently conjugated secondary antibodies diluted in blocking solution for 1 h at room temperature: donkey anti-mouse Alexa Fluor-594 (1:200 dilution, Invitrogen), donkey anti-rabbit PerCP-Cy5.5 (1:300 dilution, Santa Cruz), and donkey anti-goat Alexa Fluor-488 (1:200 dilution, Invitrogen). Nuclei were labeled with DAPI and slides coverslipped with fluorescent mounting medium (Dako). Multispectral epifluorescent images were acquired (Nuance) and spectrally unmixed to remove background autofluorescence. A total of 3 high magnification images (400°) were acquired at the mesh fiber pore interface adjacent to single fibers. The total number of cells co-expressing CD68 and either CD86 or CD206 was automatically quantified for each image using CellProfiler software (http://www.cellprofiler.org, [28]). Macrophages were defined as CD68 positive colocalized with nuclei. M1 and M2 cells were defined as macrophages coexpressing CD86 or CD206, respectively. A subpopulation of cells co-expressed both M1 and M2 markers and were subsequently denoted as “co-labeled”. Macrophage spatial distribution relative to mesh fibers was characterized by defining concentric rings around mesh fibers that were evenly spaced at 33 μm intervals. A total of 4 ring areas were defined around single fibers. Cells on the border of 2 rings were counted towards the inner ring.

2.6. Quantitative histologic analysis

A previously described [24] quantitative histomorphometric scoring system was used to evaluate the host response to the implanted mesh materials 14 an 180 days post implantation as summarized in Table 1. Fixed mesh-tissue explants were embedded in paraffin, sectioned (5 μm), mounted onto microscope slides, and stained with hematoxylin and eosin (H&E). A total of 6 high magnification images (400°) were acquired for each H&E stained section; three images of the mesh fiber/tissue interface and three images of the deposited tissue between mesh fibers. The mesh fiber/tissue interface images were positioned at the edge of mesh fiber bundles such that the inflammatory response to the mesh was visible within the field of view. The mesh fiber/tissue interface images were quantified for two criteria: the thickness of the dense cell accumulation at the fiber surface (reported as number of cell layers away from the mesh fiber) and the total number of multinucleate foreign body giant cells surrounding the mesh fiber in each image. The images of the tissue between mesh fibers were acquired at the midpoint between adjacent mesh fiber bundles and were quantified for two criteria; the total number of mononuclear cells per image (rounded to the nearest 50) and the total number of blood vessels (with identifiable lumen and red blood cells). All quantitative analysis was conducted by five (5) independent blinded observers.

2.7. Collagen quantification and characterization

The area of collagen fibers as a function of their color hue was quantified from tissue sections stained with picrosirius red and imaged with circularly polarized light microscopy (200× magnifications), as previously described [24]. The color hue corresponds to relative fiber thickness from thin green fibers to increasingly thick yellow, orange, and red fibers.

Following a previously published protocol [29,30] custom algorithmwas constructed with Matlab software (The Mathworks, Natick, MA) that: (1) cropped each image to only connective tissue directly between mesh fibers removing all subcutaneous connective and underlying muscle tissue; (2) transformed each image from the RGB to the HSV color model; (3) separated each color component as a function of hue (red 2–9 and 230–256, orange 10–38, yellow 39–51, green 52–128); (4) applied a threshold to remove noise from an average of a global threshold using Otsu's method (intensity value of 50/256); and (5) expressed the collagen content for each color component as a percentage of the area of each image.

2.8. Planar biaxial mechanical testing

Planar biaxial mechanical testing was performed as previously described [24]. Briefly, a 15 mm × 15 mm sample was acquired from each explant centered on the muscle defect. Thickness was measured from the center of each explant using a Sterret® caliper model 1010. Four (4) fiducial markers were placed in the center of the square on the anterior surface after the removal of excess loose connective tissue and fat. Deformations were measured optically by tracking this four marker array. Two loops of suture of equal length were attached to each side of the specimens with four stainless steel hooks, and 500 g Model 31 load cells (Honeywell) were used to acquire load values. Biaxial testing was conducted with the circumferential and longitudinal specimen axes aligned with the device axis and submerged in a bath at room temperature. The biaxial testing system was automated, allowing the marker locations and axial forces to be continuously recorded with custom marker tracking and data acquisition software [31].

Specimens were first preconditioned by cyclically loading the specimens to the desired maximum equibiaxial stress of 85 kPA for ten cycles using a cycle time of 30 s per cycle to quantify the quasi-static response. Immediately following the preconditioning cycles, the specimen was completely unloaded and imaged in its post-preconditioned free-floating configuration. The stress–stretch plot reported in this study start from a 0.5 g preload that is referenced to the post-precondition free float state, which was used to ensure test response repeatability. The response of the eight explants was averaged after a three point linear interpolation at representative stress values and reported with standard error. Native abdominal walls were also tested for comparison. The maximum strain for each sample was then defined as the strain at the maximum tested stress of 85 kPa.

2.9. Statistical analysis

The histomorphometric data, total number of macrophages, collagen deposition, and maximum strain values are presented as the mean ± the standard error of the mean. Statistical analysis was performed using a one-way ANOVA evaluating each variable (M1, M2, blood vessels, etc.) within each time point using SPSS software. A post-hoc Tukey test was conducted with a p-value <0.05 considered statistically significant. Data normality was determined using the Kolmgorov–Smirnov test, and natural logarithm transformation applied when normality was violated.

3. Results

After 14 days, fewer cells were present directly adjacent to and between mesh fibers in the ECM coated devices compared to the uncoated mesh devices (Figs. 3 and 4). In addition, the ECM coating resulted in a decreased number of pro-inflammatory M1 macrophages directly around the mesh fibers in comparison to the uncoated mesh devices (Fig. 5). Histomorphologic analysis at 180 days showed the ECM coating reduced the total cellularity as well as the number of foreign body giant cells around mesh fibers for the heavy-weight BARD™ mesh (Fig. 4). The ECM coating decreased the density and size of collagen deposited between mesh fibers when compared to the uncoated mesh devices (Fig. 6) at 180 days. Lastly, biaxial testing showed the ECM coating did not affect longitudinal or circumferential strain (Fig. 7).

3.1. Histologic scoring of host response around mesh fibers

Cellular accumulation and number of foreign body giant cells around mesh fibers were quantified for each mesh device 14 and 180 days post implantation (Fig. 4a, b). The ECM coating decreased the cellular accumulation around mesh fibers at both 14 and 180 days post implantation for the BARD™ and BARD™ Soft meshes. Furthermore, the ECM coating decreased the number of foreign body giant cells around the mesh fibers at 180 days post implantation for the BARD™ heavy-weight mesh. The UltraPro™ Mesh had a greater cellular accumulation around mesh fibers than the ECM coated BARD™ and BARD™ Soft meshes at both 14 and 180 days. The UltraPro™ mesh also had more foreign body giant cells around mesh fibers than the ECM coated BARD and ECM coated BARD Soft meshes at 14 days post implantation.

3.2. Histologic scoring of host response between mesh fibers

Cellularity and vascularity between mesh fibers were quantified for all mesh groups 14 and 180 days post implantation (Fig. 4c, d). The ECM coating decreased cellularity between mesh fibers when compared to the uncoated BARD™ and BARD™ Soft mesh devices at 14 days post implantation. No difference in cellularity between groups was observed at the 180 day time point. The uncoated BARD™ heavy-weight mesh had a greater amount of vascularity between mesh fibers than the other mesh devices 14 days post implantation. At 180 days the uncoated BARD™ heavy-weight and ECM coated BARD™ heavy-weight had more vascularity between fibers than the three light-weight mesh devices.

3.3. Macrophage phenotype at 14 days post implantation

The effect of an ECM coating on macrophage polarization was investigated using immunolabeling of CD68 + pan macrophages (M0), CD86 + pro inflammatory macrophages (M1), and CD206 + constructive remodeling macrophages (M2) (Fig. 5). The ECM coating markedly reduced the number of M1 pro-inflammatory cells directly adjacent to PP mesh fibers (within 100 microns of the mesh fiber) when compared to the uncoated polypropylene meshes. These results are in agreement with a previous study that an ECM hydrogel coating mitigates the host foreign body response to polypropylene mesh [24].

3.4. Thickness and quantification of collagen deposition

The total amount of collagen deposition was quantified for each mesh group at 180 days post implantation (Fig. 6). The ECM coating resulting in less overall collagen deposition (addition of all colors) when compared to the uncoated BARD™ and BARD™ Soft meshes. Both ECM coated meshes had more deposition of thin (green) collagen fibers compared to the uncoated BARD™ heavy-weight mesh. The ECM coated meshes also had less deposition of thick collagen fibers (displayed in red) compared to the uncoated BARD™ and BARD™ Soft Meshes.

3.5. Planar biaxial mechanical properties

Stress-strain curves were generated for all explants at 180, including native controls (Fig. 7a, b). The maximum strain defined at a stress of 85 kPa for both circumferential and longitudinal axis was performed for all mesh explant groups and compared to native tissue (Fig. 7c). No difference was observed between any of the mesh explant groups for both the longitudinal and circumferential maximum strains (Fig. 7c). All mesh explant groups were less compliant than native abdominal wall tissue in both circumferential and longitudinal axis.

4. Discussion

The present study showed a clear and distinct long term effect upon the host response to a PP mesh when an ECM hydrogel coating was applied. The most notable changes were the decrease in M1 pro-inflammatory macrophages around mesh fibers shortly after implantation, the decreased density of collagen, and the thinner collagen fiber type deposited between mesh fibers 180 days post implantation. The ECM hydrogel coating also decreased cellular accumulation around polypropylene mesh fibers and decreased the number of foreign body giant cells around the BARD™ heavy-weight mesh. Planar biaxial mechanical testing showed the ECM coating did not affect mesh/tissue strength at six months. These results are consistent with a previous study showing an ECM coating for a PP mesh can modulate the acute (35 day) response [24]. The present study extends the findings of the downstream remodeling outcome to 180 days following implantation of an ECM coated PP mesh in an abdominal wall defect model.

Most surgical mesh devices used for ventral hernia repair are composed of synthetic materials such as PP. These materials have many desirable features including mechanical strength and consistency in manufacturing [4–6,8,32,33]. However, they are non-degradable permanent implants and elicit a chronic inflammatory response associated with scar tissue deposition. Dense fibrous tissue forms within and around the mesh material, which can lead to complications such as bowel obstruction, perforation, infertility, enterocutaneous fistulae, and chronic discomfort [4,33–36]. This fibrotic encapsulation is associated with long-term patient discomfort, which can lead to revision surgery and surgical mesh removal [33,37]. Thus, decreasing scar tissue deposition and mitigating chronic inflammation to polypropylene would have a significant clinical impact.

Several strategies have been investigated to minimize the fibrotic response to synthetic mesh materials including alterations in the mesh fiber composition, reduction of mesh surface area (referred to as a “light-weight” mesh) and application of bioactive coatings. These approaches have been successful, but additional improvements such as an ECM hydrogel coating that can abrogate the pro-inflammatory response and associated scar tissue deposition would be desirable.

When using an ECM scaffold, site appropriate formation of functional tissue has been shown for a variety of anatomic locations including dermis, esophagus [38–40], skeletal muscle [41–43], heart, and temporomandibular joint meniscus [44], among others. There is evidence for three mechanisms by which ECM scaffolds support constructive remodeling: (i) bioactive cryptic peptides generated as a result of scaffold degradation, (ii) recruitment of endogenous stem and progenitor cells to the site of ECM remodeling, and (iii) modulation of the host immune response toward an M2-Th2 phenotype. The specific cell signaling events by which ECM biomaterials modulate the host macrophage population toward a more constructive remodeling phenotype are not fully understood. However, the phenotypic profile of macrophages that respond to these scaffold materials at early time points has been shown to be a strong predictor of the downstream tissue remodeling outcome. For example, modification of such scaffold materials with chemical cross-linking agents which delay or prevent macrophage-mediated degradation inhibits the formation of the M2 response, promotes the M1 response, and results in downstream scar tissue formation and a persistent foreign body response.

Results from the present study support the association of macrophage phenotype with remodeling. Coating polypropylene with ECM hydrogel decreased the M1 pro-inflammatory response and foreign body reaction at 14 days, which in turn was associated with decreased amount of mature collagen deposition at 180 days. UltraPro was included in this study primarily as a clinical benchmark for light-weight, partially degradable synthetic materials. UltraPro consists of a non-degradable polypropylene component and a degradable component, monocryl. Though mesh geometries differ, the analogy would be as follows: a polypropylene mesh base with a degradable component, either ECM coating, or monocryl (as polyester co-polymer). Thus the host response to both the ECM coated mesh and UltraPro is the sum of the response to two different materials, polypropylene and ECM or Monocryl. In the present study, UltraPro highlights that simply adding a degradable component, such as monocryl, is not sufficient to positively affect the host response. In fact, acidic degradation products may exacerbate the inflammatory response over time.

The promising findings of the present study allow speculation regarding the extension of an ECM coating to other biomaterial and therapeutic applications. For example, applying an ECM coating to synthetic materials used as cardiovascular stents could mitigate the subsequent intimal hyperplasia and chronic inflammatory response.

There are several key variables associated with manufacturing the ECM hydrogel coating that can be systematically addressed to further improve outcomes. For example, source animal age of the ECM has been shown to affect the in vivo remodeling characteristics. Scaffolds derived from younger animals were associated with a more constructive, site

appropriate, tissue remodeling response than scaffolds derived from older animals [45]. In addition, ECM concentration of the hydrogel should be optimized.

5. Conclusions

The present study confirms and extends previous findings that an ECM coating of a synthetic surgical mesh material can mitigate the foreign body response and associated fibrous connective tissue deposition that is characteristic of these materials. Importantly, this study demonstrates that these beneficial results persist beyond the acute timeframe and ultimately result in a more constructive tissue deposition. Specifically, the ECM coating decreases pro-inflammatory M1 macrophages at 14 days, which is associated with decreased collagen deposition at 180 days. These findings are promising and may lead to improved clinical outcomes in other regenerative medicine and biomaterial applications.

Acknowledgments

Denver Faulk was partially supported by a grant from the National Institute on Alcohol Abuse and Alcoholism (NIH 1F31AA021324-01), the National Science Foundation Graduate Research Fellowship, and the ARCS foundation. Matthew Wolf was partially supported by the NIH-NHLBI training grant (T32-HL76124-6) entitled “Cardiovascular Bioengineering Training Program” through the University of Pittsburgh Department of Bioengineering. Christopher Carruthers was partially supported by the National Science Foundation Graduate Research Fellowship. The authors would like to thank Deanna Rhoads and the McGowan Histology Center for histologic section preparation and the center for Biologic Imaging at the University of Pittsburgh for access to imaging facilities. Partial funding of this study was provided by CR Bard, Inc.

References

1. Shankaran V, Weber DJ, Reed RL 2nd, Luchette FA. A review of available prosthetics for ventral hernia repair. Ann Surg. 2011; 253(1):16–26. [PubMed: 21135699]
2. Cevasco M, Itani KM. Ventral hernia repair with synthetic, composite, and biologic mesh: characteristics, indications, and infection profile. Surg Infect. 2012; 13(4):209–15.
3. Cobb WS, Kercher KW, Heniford BT. Laparoscopic repair of incisional hernias. Surg Clin North Am. 2005; 85(1):91–103. [PubMed: 15619531]
4. Klosterhalfen B, Junge K, Klinge U. The lightweight and large porous mesh concept for hernia repair. Expert Rev Med Devices. 2005; 2(1):103–17. [PubMed: 16293033]
5. Hernandez-Gascon B, Pena E, Melero H, Pascual G, Doblare M, Ginebra MP, et al. Mechanical behaviour of synthetic surgical meshes: finite element simulation of the herniated abdominal wall. Acta Biomater. 2011; 7(11):3905–13. [PubMed: 21763794]
6. Chu CC, Welch L. Characterization of morphologic and mechanical properties of surgical mesh fabrics. J Biomed Mater Res. 1985; 19(8):903–16. [PubMed: 3880350]
7. Ozog Y, Konstantinovic M, Werbrouck E, De Ridder D, Mazza E, Deprest J. Persistence of polypropylene mesh anisotropy after implantation: an experimental study. BJOG. 2011; 118(10): 1180–5. [PubMed: 21668770]
8. Feola A, Barone W, Moalli P, Abramowitch S. Characterizing the ex vivo textile and structural properties of synthetic prolapse mesh products. Int Urogynecol J. 2013; 24(4):559–64. [PubMed: 22885725]
9. Bello YM, Falabella AF, Eaglstein WH. Tissue-engineered skin. Current status in wound healing. Am J Clin Dermatol. 2001; 2(5):305–13. [PubMed: 11721649]
10. Butler CE, Langstein HN, Kronowitz SJ. Pelvic, abdominal, and chest wall reconstruction with AlloDerm in patients at increased risk for mesh-related complications. Plast Reconstr Surg. 2005; 116(5):1263–75. discussion 76–77. [PubMed: 16217466]

11. Franklin ME Jr, Gonzalez JJ Jr, Glass JL. Use of porcine small intestinal submucosa as a prosthetic device for laparoscopic repair of hernias in contaminated fields: 2-year follow-up. Hernia. 2004; 8(3):186–9. [PubMed: 14991410]
12. Badylak SF. The extra-cellular matrix as a biologic scaffold material. Biomaterials. 2007; 28(25): 3587–93. [PubMed: 17524477]
13. Hodde J, Hiles M. Constructive soft tissue remodelling with a biologic extracellular matrix graft: overview and review of the clinical literature. Acta Chir Belg. 2007; 107(6):641–7. [PubMed: 18274177]
14. Sikkink CJ, Zeebregts CJ, Reijnen MM. Hyaluronan-based antiadhesive agents in abdominal surgery: applications, results, and mechanisms of action. Surg Technol Int. 2007; 16:19–29. [PubMed: 17429764]
15. Sicari BM, Zhang L, Londono R, Badylak SF. An assay to quantify chemotactic properties of degradation products from extracellular matrix. Methods Mol Biol. 2014; 1202:103–10. [PubMed: 24155230]
16. Tottey S, Corselli M, Jeffries EM, Londono R, Peault B, Badylak SF. Extracellular matrix degradation products and low-oxygen conditions enhance the regenerative potential of perivascular stem cells. Tissue Eng Part A. 2011; 17(1–2):37–44. [PubMed: 20653348]
17. Brennan EP, Tang XH, Stewart-Akers AM, Gudas LJ, Badylak SF. Chemo-attractant activity of degradation products of fetal and adult skin extracellular matrix for keratinocyte progenitor cells. J Tissue Eng Regen Med. 2008; 2(8):491–8. [PubMed: 18956412]
18. Reing JE, Zhang L, Myers-Irvin J, Cordero KE, Freytes DO, Heber-Katz E, et al. Degradation products of extracellular matrix affect cell migration and proliferation. Tissue Eng Part A. 2009; 15(3):605–14. [PubMed: 18652541]
19. Brennan EP, Reing J, Chew D, Myers-Irvin JM, Young EJ, Badylak SF. Antibacterial activity within degradation products of biological scaffolds composed of extracellular matrix. Tissue Eng. 2006; 12(10):2949–55. [PubMed: 17518662]
20. Ramchandran R, Dhanabal M, Volk R, Waterman MJ, Segal M, Lu H, et al. Antiangiogenic activity of restin, NC10 domain of human collagen XV: comparison to endostatin. Biochem Biophys Res Commun. 1999; 255(3):735–9. [PubMed: 10049780]
21. Valentin JE, Turner NJ, Gilbert TW, Badylak SF. Functional skeletal muscle formation with a biologic scaffold. Biomaterials. 2010; 31(29):7475–84. [PubMed: 20638716]
22. Wolf MT, Daly KA, Brennan-Pierce EP, Johnson SA, Carruthers CA, D'Amore A, et al. A hydrogel derived from decellularized dermal extracellular matrix. Biomaterials. 2012; 33(29): 7028–38. [PubMed: 22789723]
23. Badylak SF, Freytes DO, Gilbert TW. Extracellular matrix as a biological scaffold material: structure and function. Acta Biomater. 2009; 5(1):1–13. [PubMed: 18938117]
24. Wolf MT, Carruthers CA, Dearth CL, Crapo PM, Huber A, Burnsed OA, et al. Polypropylene surgical mesh coated with extracellular matrix mitigates the host foreign body response. J Biomed Mater Res A. 2013; 102(1):234–46. [PubMed: 23873846]
25. Valentin JE, Badylak JS, McCabe GP, Badylak SF. Extracellular matrix bioscaffolds for orthopaedic applications. A comparative histologic study. J Bone Jt Surg Am. 2006; 88(12):2673–86.
26. Brown BN, Londono R, Tottey S, Zhang L, Kukla KA, Wolf MT, et al. Macrophage phenotype as a predictor of constructive remodeling following the implantation of biologically derived surgical mesh materials. Acta Biomater. 2012; 8(3):978–87. [PubMed: 22166681]
27. Freytes DO, Martin J, Velankar SS, Lee AS, Badylak SF. Preparation and rheological characterization of a gel form of the porcine urinary bladder matrix. Biomaterials. 2008; 29(11): 1630–7. [PubMed: 18201760]
28. Carpenter AE, Jones TR, Lamprecht MR, Clarke C, Kang IH, Friman O, et al. CellProfiler: image analysis software for identifying and quantifying cell phenotypes. Genome Biol. 2006; 7(10):R100. [PubMed: 17076895]
29. Whittaker P, Kloner RA, Boughner DR, Pickering JG. Quantitative assessment of myocardial collagen with picrosirius red staining and circularly polarized light. Basic Res Cardiol. 1994; 89(5):397–410. [PubMed: 7535519]

30. Nadkarni SK, Pierce MC, Park BH, de Boer JF, Whittaker P, Bouma BE, et al. Measurement of collagen and smooth muscle cell content in atherosclerotic plaques using polarization-sensitive optical coherence tomography. J Am Coll Cardiol. 2007; 49(13):1474–81. [PubMed: 17397678]
31. Billiar KL, Sacks MS. Biaxial mechanical properties of the natural and glutar-aldehyde treated aortic valve cusp–Part I: experimental results. J Biomech Eng. 2000; 122(1):23–30. [PubMed: 10790826]
32. Cobb WS, Kercher KW, Heniford BT. The argument for lightweight poly-propylene mesh in hernia repair. Surg Innov. 2005; 12(1):63–9. [PubMed: 15846448]
33. Klinge U, Klosterhalfen B, Muller M, Schumpelick V. Foreign body reaction to meshes used for the repair of abdominal wall hernias. Eur J Surg. 1999; 165(7):665–73. [PubMed: 10452261]
34. Leber GE, Garb JL, Alexander AI, Reed WP. Long-term complications associated with prosthetic repair of incisional hernias. Arch Surg. 1998; 133(4):378–82. [PubMed: 9565117]
35. Di Vita G, D'Agostino P, Patti R, Arcara M, Caruso G, Davi V, et al. Acute inflammatory response after inguinal and incisional hernia repair with implantation of polypropylene mesh of different size. Langenbecks Arch Surg. 2005; 390(4):306–11. [PubMed: 15690201]
36. Garcia-Urena MA, Vega Ruiz V, Diaz Godoy A, Baez Perea JM, Marin Gomez LM, Carnero Hernandez FJ, et al. Differences in polypropylene shrinkage depending on mesh position in an experimental study. Am J Surg. 2007; 193(4):538–42. [PubMed: 17368306]
37. Costello CR, Bachman SL, Ramshaw BJ, Grant SA. Materials characterization of explanted polypropylene hernia meshes. J Biomed Mater Res B Appl Biomater. 2007; 83(1):44–9. [PubMed: 17285608]
38. Nieponice A, McGrath K, Qureshi I, Beckman EJ, Luketich JD, Gilbert TW, et al. An extracellular matrix scaffold for esophageal stricture prevention after circumferential EMR. Gastrointest Endosc. 2009; 69(2):289–96. [PubMed: 18657808]
39. Badylak SF, Vorp DA, Spievack AR, Simmons-Byrd A, Hanke J, Freytes DO, et al. Esophageal reconstruction with ECM and muscle tissue in a dog model. J Surg Res. 2005; 128(1):87–97. [PubMed: 15922361]
40. Badylak S, Meurling S, Chen M, Spievack A, Simmons-Byrd A. Resorbable bioscaffold for esophageal repair in a dog model. J Pediatr Surg. 2000; 35(7):1097–103. [PubMed: 10917304]
41. Turner NJ, Badylak JS, Weber DJ, Badylak SF. Biologic scaffold remodeling in a dog model of complex musculoskeletal injury. J Surg Res. 2012; 176(2):490–502. [PubMed: 22341350]
42. Sicari BM, Rubin JP, Dearth CL, Wolf MT, Ambrosio F, Boninger M, et al. An acellular biologic scaffold promotes skeletal muscle formation in mice and humans with volumetric muscle loss. Sci Transl Med. 2014; 6(234):234ra58.
43. Mase VJ Jr, Hsu JR, Wolf SE, Wenke JC, Baer DG, Owens J, et al. Clinical application of an acellular biologic scaffold for surgical repair of a large, traumatic quadriceps femoris muscle defect. Orthopedics. 2010; 33(7):511. [PubMed: 20608620]
44. Brown BN, Chung WL, Pavlick M, Reppas S, Ochs MW, Russell AJ, et al. Extracellular matrix as an inductive template for temporomandibular joint meniscus reconstruction: a pilot study. J Oral Maxillofac Surg. 2011; 69(12):e488–505. [PubMed: 21684655]
45. Sicari BM, Johnson SA, Siu BF, Crapo PM, Daly KA, Jiang H, et al. The effect of source animal age upon the in vivo remodeling characteristics of an extra-cellular matrix scaffold. Biomaterials. 2012; 33(22):5524–33. [PubMed: 22575834]

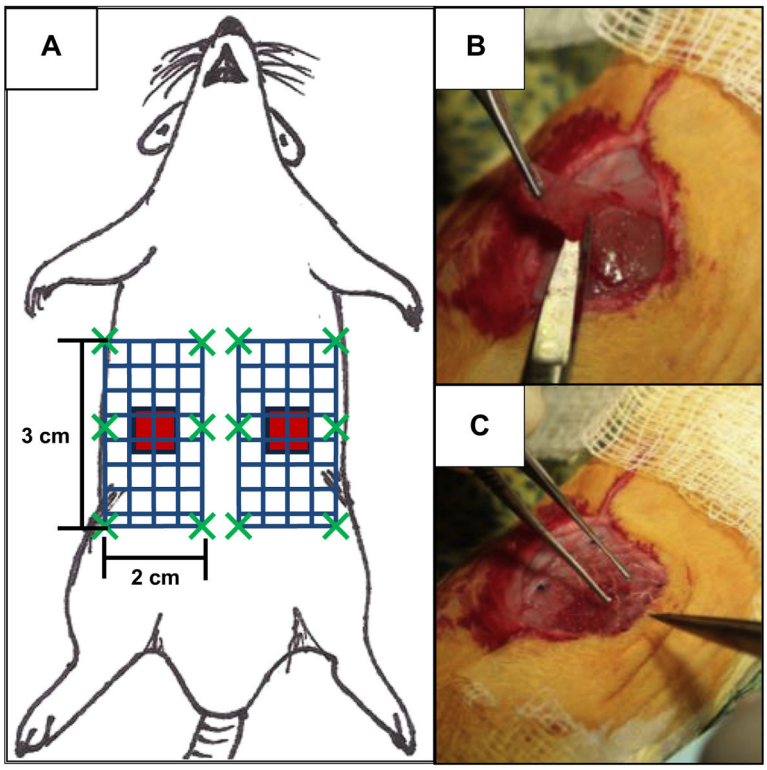

Fig. 1.

Surgical model of mesh implantation in a rat. (A) Schematic representation of mesh placement. Two 1 cm × 1 cm partial thickness abdominal wall paramedian defects were created (red squares), and were repaired with 2 cm × 3 cm mesh devices (blue patterned rectangle) using an overlay technique. Each mesh was parallel to the midline and bordered the edge of the rectus abdominus. Mesh devices were fixed to the abdominal using six single interrupted sutures (dark green "X"s) along the edge of the mesh. (B) The 1 cm × 1 cm partial thickness defect was created by removing the internal and external oblique, leaving the transversalis fascia and the peritoneum intact. (C) After making the defect, the 2 cm× 3 cm surgical mesh test article was then fixated directly over top of the defect. (For interpretation of the references to color in this figure legend, the reader is referred to the web version of this article.)

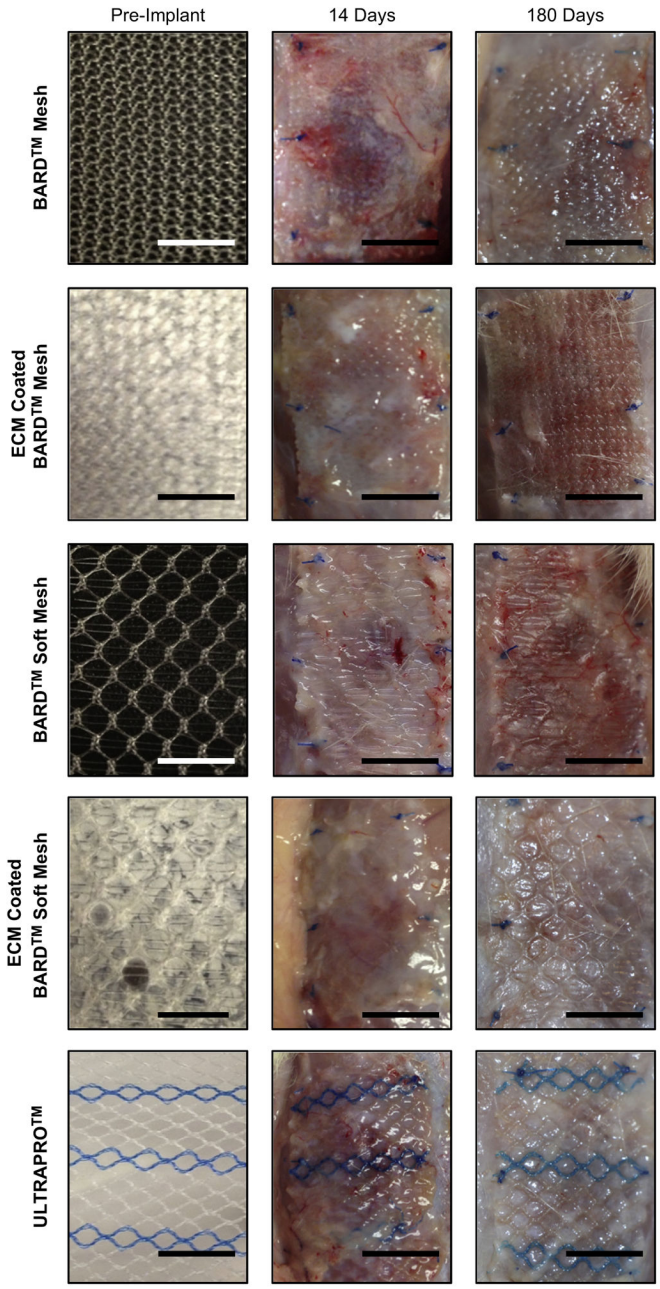

Fig. 2.

Macroscopic images of each mesh device pre-implant (left column), 14 days post implantation (middle column), and 180 days post implantation (right column). Scale bar = 1 cm.

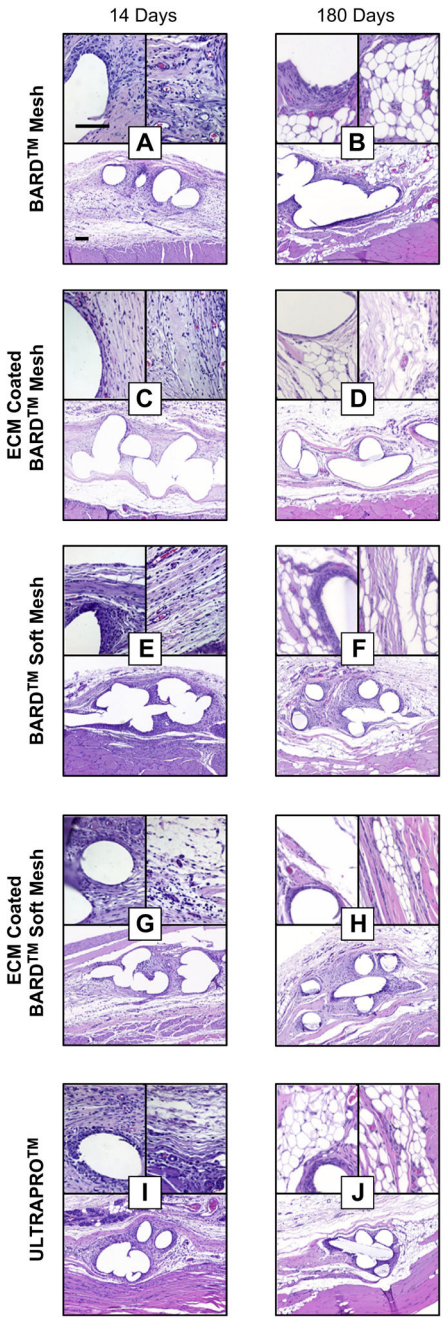

Fig. 3.

Histologic appearance of mesh devices after 14 and 180 days of in vivo implantation. Representative H&E stained histologic cross sections of each mesh/time point were imaged at 100× magnification (bottom of each figure panel) and 400× magnification (top two images of each figure panel) Scale bars represent 100 μm.

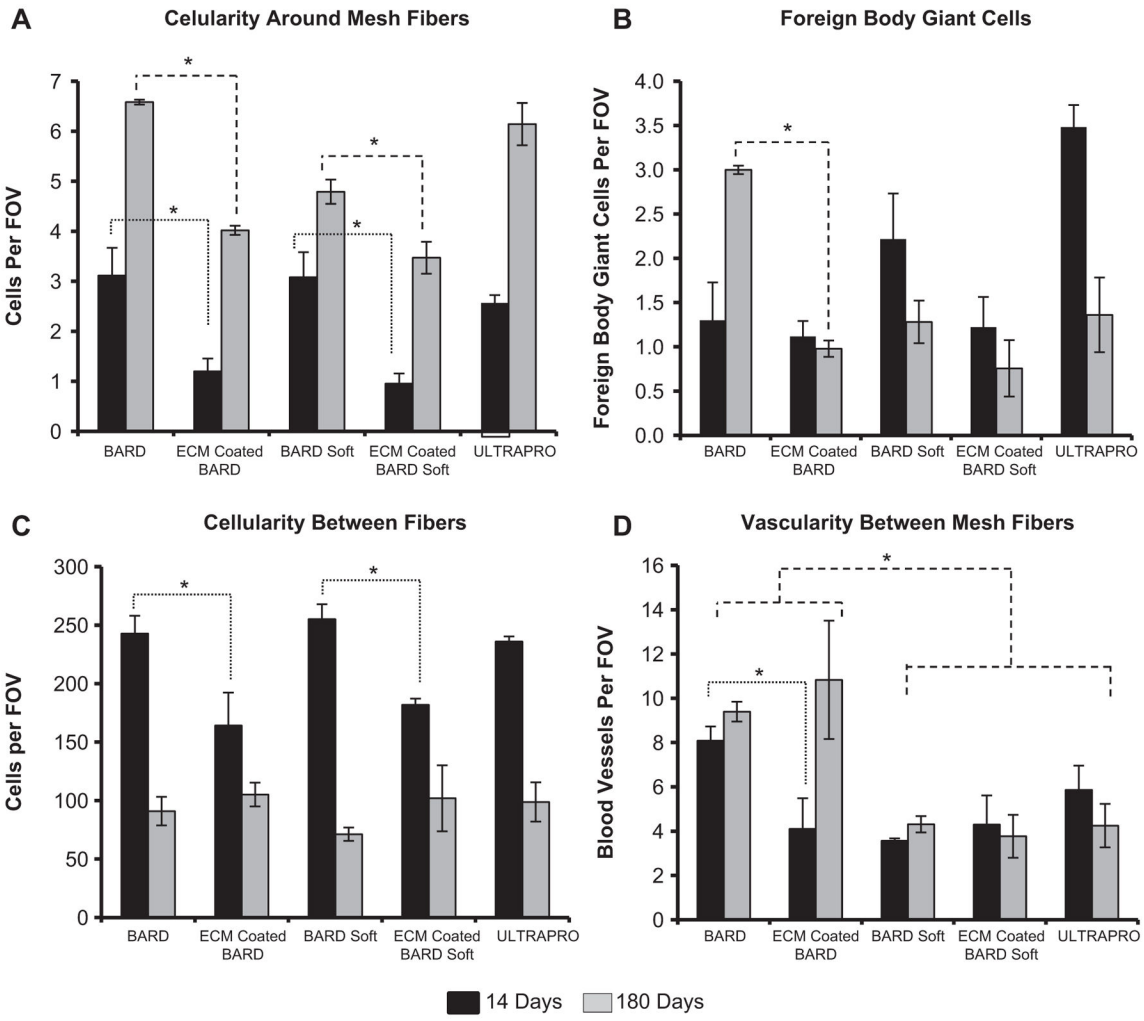

Fig. 4.

Histomorphometric analysis of the histologic inflammatory response to mesh fibers and tissue remodeling in the area between mesh fibers from H&E stained histologic cross sections after 14 and 180 days post-implantation. (A) The mesh fiber cellularity and (B) number of foreign body giant cells for each device were counted to characterize the inflammatory response to mesh fibers. Tissue remodeling between mesh fibers was analyzed as the (C) number cells and (D) number of blood vessels. Significant differences ($p < 0.05$) between devices within each time point are denoted as (*).

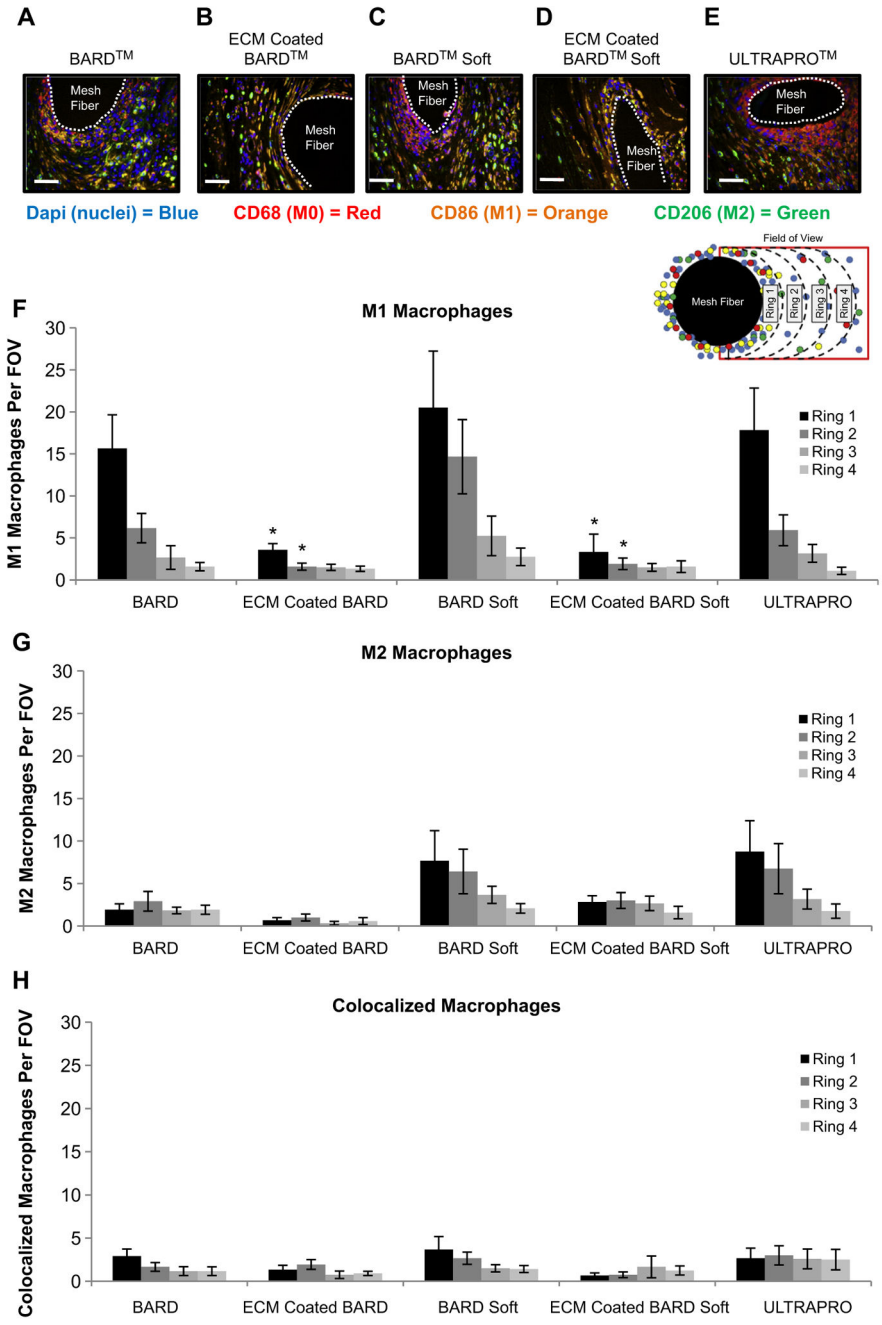

Fig. 5.

(A–E) Representative immunofluorescent images of the host macrophage response to mesh materials at 14 days post-implantation. Dapi (nuclei) = blue, CD68 (M0) = Red, CD86 (M1) = Orange, CD206 (M2) = Green. Quantification of the (F) pro-inflammatory M1 (CD86+/CD68+) macrophages, (G) constructive remodeling M2 (CD206+/CD68+) macrophages, and (H) colocalized (CD86+/CD206+/CD68+) near mesh fibers. Each ring (1–4) represents increasing distance from the mesh fiber surface. Scale bar = 50 μm. (For interpretation of the references to color in this figure legend, the reader is referred to the web version of this article.)

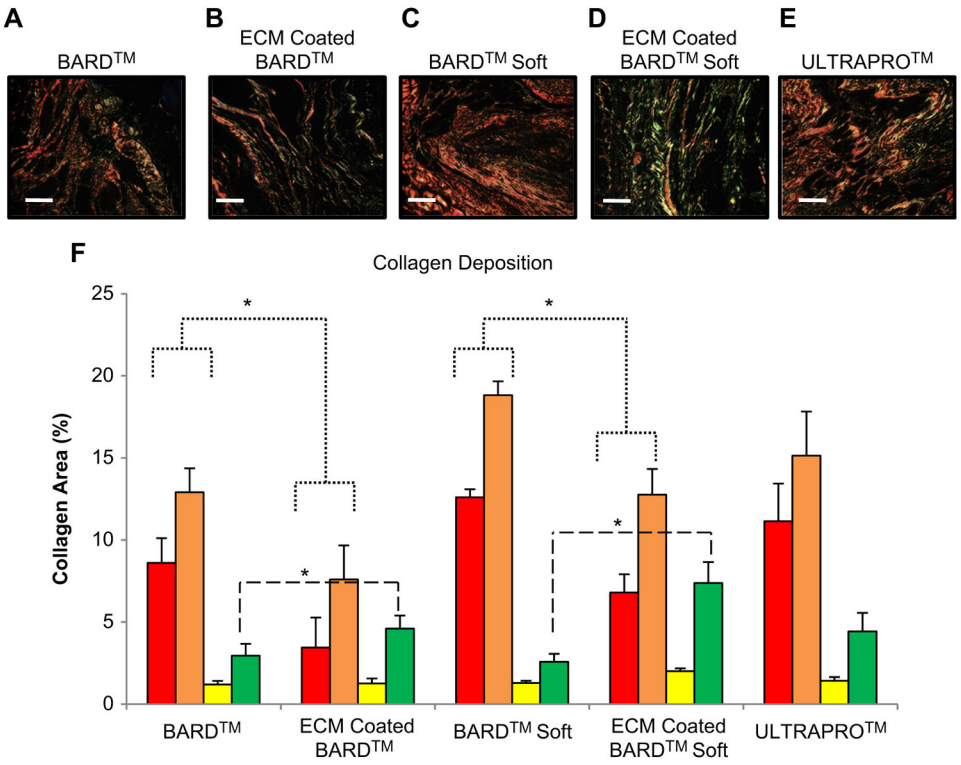

Fig. 6.

Picrosirius red staining and quantification of collagen area between mesh fibers using polarized light microscopy. (A–E) Collagen fibers between the mesh fibers of each device after 180 days. The color hue of the fibers represents the relative collagen thicknesses (in order of thinnest to thickest): green, yellow, orange, and red. (F) Quantification of the total area and proportion of collagen (defined by color hue) in each mesh after 180 days. Significant differences ($p < 0.05$) are denoted (*). Scale bar represents 50 μm. (For interpretation of the references to color in this figure legend, the reader is referred to the web version of this article.)

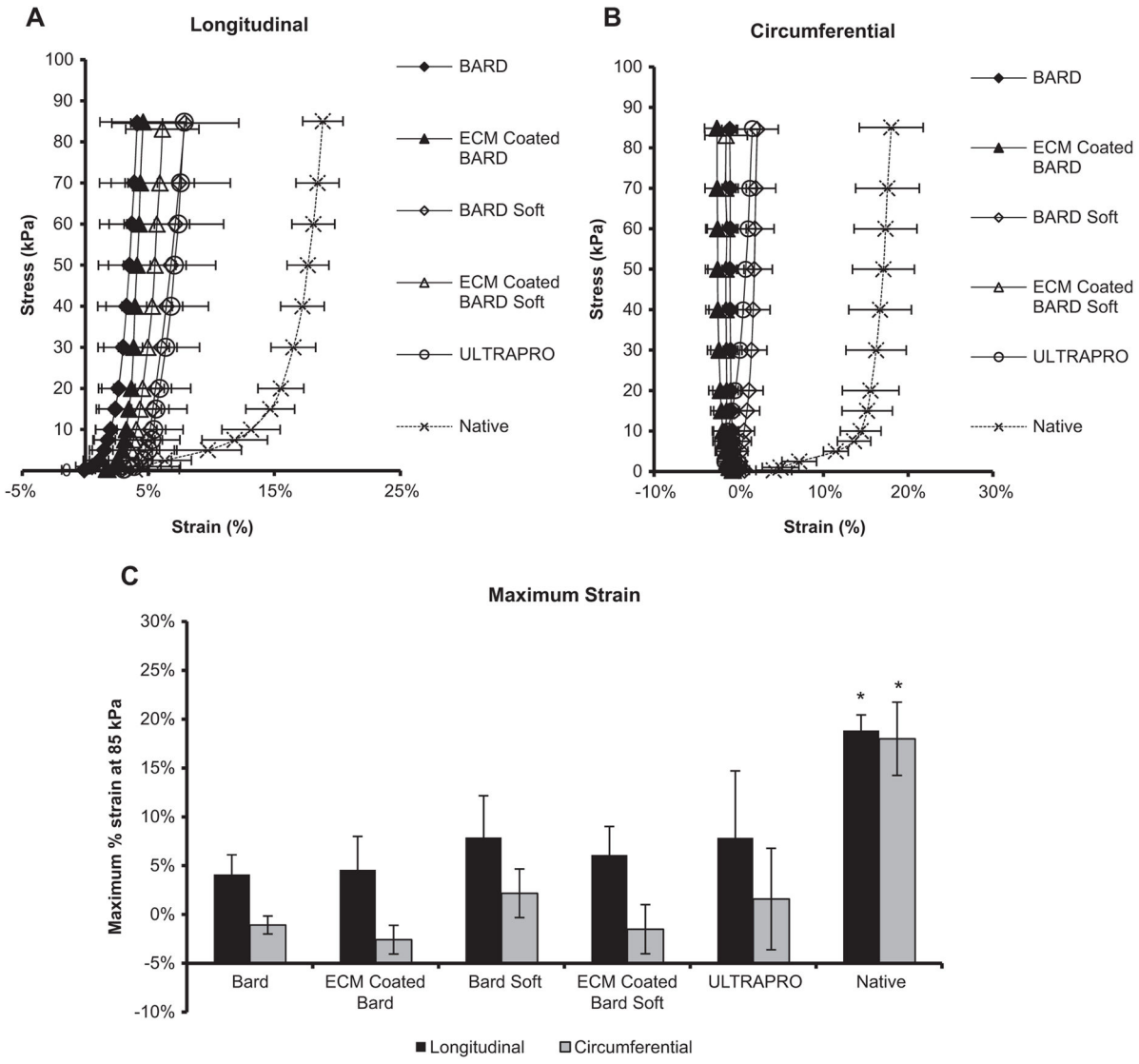

Fig. 7.

Mesh explants equibiaxial mechanical characterization after 180 days. (A) The equibiaxial stress response of the explanted mesh devices were characterized along the circumferential and (B) longitudinal axes. (C) The maximum strain defined at a stress of 85 kPa for both circumferential and longitudinal axes. Significant differences ($p < 0.05$) are denoted (*).

Table 1

Summary of quantitative histomorphometric analysis categories.

Location of analysis	Analysis	Description of quantitative analysis
Around mesh fibers	Cellularity	Number of cell layers of dense cellular accumulation immediately adjacent to fibers per field of view
	Foreign body giant cells	Number of foreign body giant cells per field of view
Between mesh fibers	Cellularity	Number of mononuclear cells per field of view in increments of 50 cells
	Vascularity	Number of blood vessels per field of view